HIghly advanced Probabilistic design and Enhanced Reliability methods for high-value, cost-efficient offshore WIND

Title: Floating wind turbine structural design procedure including SLS

Deliverable no: D4.4

Delivery date:

Lead beneficiary: DTU

Dissemination level: Public

This project has received funding from the European Union's Horizon 2020 Research and Innovation Program under Grant Agreement No. 101006689

Author information (alphabetical):		
Name	Organization	Email
B. Yildirim	DTU	bysyi@dtu.dk
N. Dimitrov	DTU	nkdi@dtu.dk

Acknowledgements/Contributions::		
Name	Name	Name

Document information:					
Version	Date	Description	Prepared by	Reviewed by	Approved by
1.0	30.09.2024	Official	Authors listed above	Yann Poirette Henrik Bredmose	A. Kolios

Definition:	

Contents

List of Figures

List of Tables

List of Abbreviations

ALS	Accidental Limit State
CCD	Central Composite Design
DEL	Damage Equivalent Load
DLB	Design Load Basis
DLC	Design Load Case
DOE	Design of Experiment
ECM	Extreme Current Model
ETM	Extreme Turbulence Model
FLS	Fatigue Limit State
FWT	Floating Wind Turbine
IEA	International Energy Agency
IEC	International Electrotechnical Commission
MSL	Mean Sea Level
NCM	Normal Current Model
NTM	Normal Turbulence Model
OWF	Offshore Wind Farm
RNA	Rotor Nacelle Assembly
SCF	Stress Concentration Factor
SKS	Station Keeping System
SLS	Serviceability Limit State
SWL	Still Water Level
ULS	Ultimate Limit State
WP	Work package

1 Executive Summary

This report discusses the design challenges and practices for floating wind turbines (FWTs). It outlines a FWT design procedure which calculates the impact of modifying floater dimensions on FWT design limit states, including ULS, FLS, and SLS (Ultimate, Fatigue, and Serviceability Limit States respectively). It also includes considerations on other variables characteristic of, or linked to floater behaviour such as tower top acceleration, floater offset, and blade clearance. A path towards a complete probabilistic design framework for FWT is laid out, and as a preliminary step, a design sensitivity analysis is carried out. Model input uncertainties both on environmental conditions and on the design of a FWT are investigated. The details of the sections are given below:

Problem formulation and introduction to the problem (Section 2): this section outlines the current state-of-the-art and challenges in FWT design applications, to provide insights into the requirements for a design framework, and define related focal points. To specify a comprehensive definition, the design optimization and reliability-based design applications for OWTs are presented and finally, the objectives of this study are given.

Case Study Description (Section 3): The case study for the application of the methodology is presented. The details of the turbine, floater, and station-keeping system are described. Environmental conditions of the selected site are given with the selected distributions and parameters.

Sensitivity analysis using an automated design evaluation framework (Section 4): This section describes the proposed structural design evaluation procedure for FWTs which considers the dimensions of the floater and the station-keeping system. Selection of the design of the experiment (DOE), floater parameterization, and design evaluation process are provided. Preparation of the aeroelastic, hydrodynamic, and mooring model for the FWT system is described.

Serviceability Limit State Assessment (Section 5): Relevant Serviceability limit states for the floater are discussed.

Case Demonstration (Section 6): Outputs of the DLB (Design Load Basis) simulations for the reference design concept are presented for FLS and ULS conditions. SLS evaluation is also conducted indicating the specific DLCs (Design Load Cases) for SLS.

Conclusion (Section 7): Discussion of the sensitivity analysis for the automated design procedure is addressed and details of the automated design evaluation framework are presented. Recommendations for the SLS are discussed.

2 Introduction and problem formulation

2.1 State-of-the-art and challenges in FOWT design optimization

Floating Offshore Wind Turbines (FOWT) operate in a challenging marine environment. This needs to be taken into account in the design procedure in order to ensure the integrity of the structures throughout their entire design lifetime. In comparison to most other offshore structures, however, FOWTs have the additional challenge of not being fixed to the seabed. The presence of a mooring system and floater motion introduces additional dynamic effects and potential failure modes. In this section, we outline the primary challenges with respect to the design and reliability of FOWTs.

Control (Negative Damping) Negative damping or floating wind turbine pitch instability problem is a known phenomenon for FWT modeling and design where for wind speeds above rated ($\approx$ 12-15m/s) the standard onshore turbine controller causes oscillations and increasing motion of the FWT system. One approach to solve this issue is to de-tune the controller which reduces the controller reaction speed and hence prevents the oscillatory motion (Larsen and Hanson, 2007). De-tuning the controller solves the instability problem. However, it results in a slow controller response, which might reduce the efficiency of energy production and load mitigation strategies. In this report, another approach is preferred which introduces tower top velocity feedback in the controller loop.

Nonlinear effects in the system Wind turbine dynamics include nonlinearities that stem from nonlinear aero- and hydro-dynamics effects, variable rotor speed, and from large structural deflections. Larger offshore turbines have longer blades and higher towers, which requires special attention with respect to nonlinear behaviour. Wind turbine structural design practices recommend using time domain methods to accommodate the non-linearities in the wind turbine system (iec, 2019). However, time domain simulations require greater computational effort compared to frequency domain approaches and are not particularly suitable for repeated design iterations. Additional issues with large blades could be caused by high flexibility which leads to large deflections and potential interference with the tower.

Uncertainties in the hydrodynamic damping during the design process Determining hydrodynamic damping is a demanding problem in hydrodynamics and especially for FWTs in extreme sea states.

Design optimization Design optimization of FWTs requires investigation of a large design space where the application of time-domain simulations can have higher computational cost and hence becomes inefficient for the design process (Ojo et al., 2021). To avoid this issue, frequency domain analysis can be used for the dynamic analysis of the structures where the frequency domain applications have some limitations including being only suitable for linear dynamic systems (Journee and Massie, 2001).

Additional design constraints The discussion of the design constraints so far has considered a single wind turbine. For realistic design optimization, the FWT system should be considered as being a part of an offshore wind farm (OWF). Moving from the component level to the OWF level, additional attention should be given to farm-level consequences including dynamic cable motion limits and wake losses due to other turbines. The allowable floater motion defined as a design constraint affects the mooring design, dynamic cable design, and the wind farm layout. Ahmad et al. (2023) implemented an optimization methodology for the dynamic cable (inter-array power cable) including the effects of marine growth and performed dynamic analysis for the selected inter-array cable designs to define the maximum offset. The maximum offset (or excursion) should be compatible with the expected floater motion. In other words, the cable should be able to accommodate the floater motion with its loose S-shape and its margin. This term is mentioned as the offset design of the dynamic cable (Taninoki et al., 2017).

In addition to the structural and operational constraints for the design of FWTs, site-specific and/or environmental constraints may be considered during the optimization process, such as clearance from the blade tip to the inspection platform. The blade tip clearance with respect to

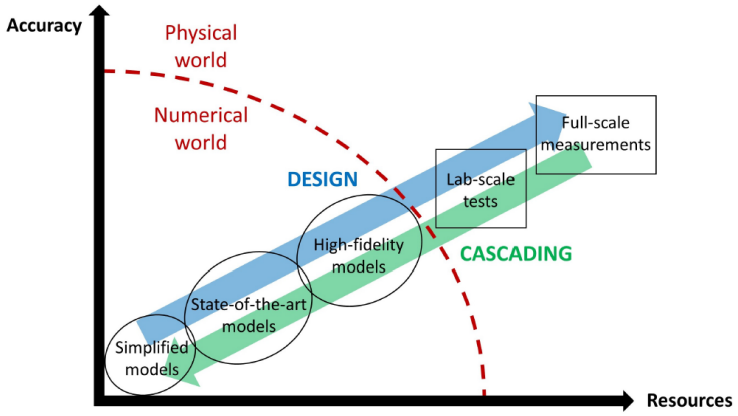

Figure 2.1: FWT modeling and design tools cascading (Pegalajar Jurado, 2018)

the water level and from the tower can be defined according to the local regulations considering bird collision protection and tidal levels.

2.2 Design optimization and reliability-based design of FOWT

From the first FWT design concept, the tools and methods have evolved following technological advancements and the increased availability of computational resources. The initial methodologies were inspired from the practices of the oil and gas industry, but the methods have further evolved with experience from the first concepts and prototypes. With the improved design practices the cost of FWTs became more competitive, yet still more work should be done to further reduce their LCOE. While for bottom fixed turbines the cost contributions from the turbine, O&M expenses, and support structure are similar, for FWTs the substructure/foundation related costs as well as the O&M costs are significantly higher (Stehly and Duffy, 2021).

The design evaluation objective for FWTs varies within the literature. To ensure safe operation, the aim is to minimize nacelle acceleration or heel angle (static displacement) of the FWT system (Pegalajar Jurado, 2018). For improving the accuracy of the design, e.g. going from conceptual design to detailed design phase, multiple modelling fidelity levels are used. An example of the modelling tool fidelities can be seen in Figure 2.1.

2.3 FOWT Design limit states

Design limit states for a structure can be divided into four classes: Serviceability limit states (SLS), Ultimate Limit States (ULS), Fatigue Limit States (FLS), and Accidental Limit States (ALS). SLS represents the limit whose non-exceedance means that the structure can continue its normal functions and operations. The exceedance of SLS does not usually imply safety issues but results in economic losses and disruption of its function (Griffis, 1993). ULS is the failure limit of the structure and substructures in terms of extreme actions. In contrast, FLS is the design limit for cyclic damage accumulation under repeated loads. Finally, ALS represents accidental events or events with very rare occurrences and harsh effects on the system (Paik and Thayamballi, 2007). Reduced load-carrying capacity including yielding and buckling, brittle fracture failure,

and excessive deformations can be considered ULS cases (GL, 2018). Considering the FWT specific limit states, loss of static equilibrium as ULS might result in the overturning of the FWT system (Cui et al., 2022). Some examples of ALS can be stated as, damage or failure due to accidental loads surpassing the ultimate resistance, or loss of structural integrity posterior to local damage (GL, 2018). Due to the proximity of the offshore wind farms to ship traffic, collisions while maneuvering can be expected, and goods or equipment might fall and hit the turbine during operation of the supply vessels (Yu et al., 2022). Ship collision is therefore a potential ALS case for any offshore wind turbine. And for FWTs specifically, the possibility of collisions with the mooring system may mean even more potential ship-related ALS cases.

Although there is a simplified analytical method for considering ship collision in terms of force and energy, it can not be used to assess the collision behaviour as energy dissipation, collision force, damage on the structure and tower motion (Song et al., 2021). This kind of assessment to capture collision behavior requires detailed simulations including collision likelihood analysis and collision damage analysis with high fidelity finite element method (FEM) approach including the technical properties of the ship and detailed structural properties of the FWT (Moulas et al., 2017). This is outside the scope of the current deliverable which focuses on the global limit states on the structure. The local and accidental limit states are not investigated further and assessment of the effects of ship collision is not included in the design evaluation process.

Existing literature indicates that there is limited knowledge on the definition of SLS for FWTs, and the concrete SLS cases are not explicitly listed or standardized across the industry. The SLS definitions are stated as project-specific in the current design guidelines. In this report, potential SLS definitions for FWTs are discussed in Section 5, and proposed SLS modes are presented in detail.

2.4 Objectives of the Present Study

The aim of the present study is to establish a robust computational procedure for FWT design evaluation with parameterized floater design characteristics. The computational framework is then utilized to carry out sensitivity analysis on how design limit states are impacted by changes in floater design parameters. This is completed through several specific goals:

- Outline the requirements for the types and extent of numerical simulations required to carry out adequate FOWT design evaluation;
- Develop a semi-automated design evaluation framework taking the said requirements into account;
- Demonstrate the design evaluation process on a realistic use case and show how different limit states are affected by design parameters;
- Outline prominent SLS, what computational approaches are needed for evaluating them, and what is the SLS sensitivity on the floater design parameters.

3 Case study description

The work in this report is based on a single virtual use case employing the International Energy Agency (IEA) 15MW reference wind turbine (Gaertner, 2020) coupled with the UMaine semi-submersible floater (Allen et al., 2020) and placed at an offshore site in South Brittany. The

reference design includes several modifications introduced in earlier HIPERWIND activities. The following sections give a brief overview of the turbine, floater and site conditions.

3.1 Turbine

The IEA 15MW reference turbine designed for IEC class 1B conditions is considered. The design information includes the rotor nacelle assembly (RNA), and the tower. A detailed design definition is available in (Gaertner, 2020) and a summary of the main properties is given in Table 3.1.

Table 3.1: IEA 15 MW Wind Turbine properties Adapted from, (Gaertner, 2020).

Parameter	Value	Units
Power Rating	15	MW
Turbine Class	IEC Class 1B	-
Specific Rating	332	W/m^2
Cut in Wind Speed	3	m/s
Rated in Wind Speed	10.59	m/s
Cut out Wind Speed	25	m/s
Rotor Diameter	240	m
Hub Height	150	m

The use case defined within the Hiperwind project accommodates modifications introduced in the previous work packages. The changes are briefly outlined here. The RNA global mass is reduced by 131 tons and for the aeroelastic models created, the shaft is modeled as a flexible beam but the hub and nacelle are implemented as lumped masses. Properties of the modified RNA can be found in Table 3.2. The tower was redesigned to avoid a resonance issue that was noticed with the original design. The tower for the FWT concept is optimized with three main criteria including a tower natural frequency distance constraint of at least 15 % from the 3P frequency, manufacturing constraints to avoid local buckling and maximum diameter variation angle of 3 degrees between the tower segments, and finally elastic behavior verification for the ULS case with 43 m/s. The detailed design of the tower can be found in previous HIPERWIND activities.

Table 3.2: Modified RNA mass and inertia properties for the Hiperwind Model

Parameter	Value (Actual)	Value (Hiperwind)	Units
Hub Mass	190000	190000	kg
Hub Inertia about rotor axis	1382171	1382171	kgm^2
Nacelle Mass	630888	430000	kg
Nacelle Inertia about Yaw axis	10046187	10046187	kgm^2

Figure 3.1: Umaine Semisubmersible with IEA 15 MW Turbine (Allen et al., 2020; Gaertner, 2020)

3.2 Floater and Station Keeping System

The reference floater in this work is based on the UMaine VolturnUS steel semisubmersible design. For the Hiperwind base case, the floater geometry was not modified. As a result of the change in water depth from 200 m (initial site Gulf of Maine) to 150 m (Hiperwind Site in South Brittany), the mooring system is adjusted to the new site, and the ballast of the system is modified to account for the design adaptations in the RNA and tower of the base case. In addition to the modifications above, the model code-to-code comparison campaign (Kim et al., 2022) revealed that the base case model is not suitable for the 50-year extreme wave conditions of South Brittany. The extreme wave conditions cause dynamic slack in the mooring lines. To resolve this issue, a modification was introduced in Hiperwind work package (WP) 3.3 (Peyrard and Robaux, 2022), by adding a clump weight of 60 tons to each mooring line from 100 m. In the present work, the final modified version is used.

3.3 Site Conditions

Identification of the accurate environmental characteristics is crucial for evaluating a design concept and its operational life. A site outside of South Brittany in western France is selected as the location of interest. 32-years of environmental data is available for the location from the ANEMOC (Digital Atlas of Ocean and Coastal Sea States) reanalysis database (Tiberi-Wadier et al., 2016). The bathymetry of the selected site and the location of interest can be seen below in Figure 3.2. Raw data from the ANEMOC database (Tiberi-Wadier et al., 2016) is prepro-

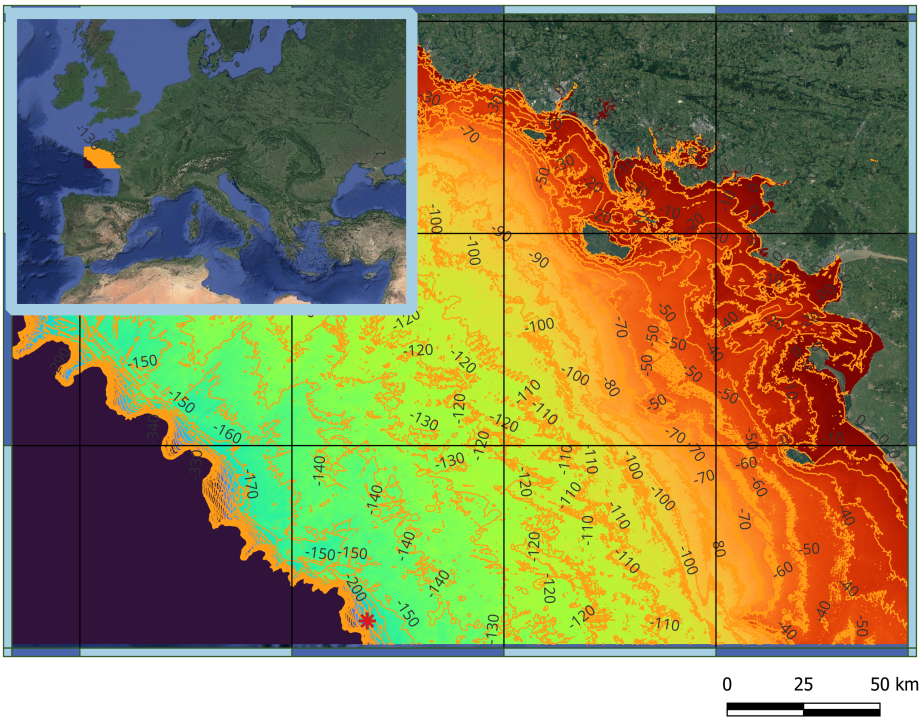

Figure 3.2: Location/Bathymetry of the selected site in South Brittany

cessed previously in the Hiperwind work packages (Vanem et al., 2023) to obtain the hourly values of mean wind speed, significant wave height, and peak wave period. In addition to this, using the power law profile (DNV, 2014) the mean wind speed at 10 m above the mean sea level is translated to hub height (U_{hub}).

$$U_{hub} = U_{ref}(\frac{z_{hub}}{z_{ref}})^{0.1}$$

In addition to the wave and wind conditions, current reanalysis data from the ANEMOC database (Tiberi-Wadier et al., 2016) is preprocessed to obtain the normal current model (NCM) and Extreme current model (ECM) for the design load basis (DLB).

For the DLB, the site-specific turbulence is not used in this work as there was no data available for it. Instead, the normal turbulence model (NTM) and extreme turbulence model (ETM) are defined based on the IEC61400-1 standard (iec, 2019) for a turbine class 1B.

4 Sensitivity analysis using an automated design evaluation framework

The design evaluation process is automated using a Python-based modelling framework. All preprocessing, calling of external executables, and postprocessing steps are carried out within the Python wrapper code. The only non-automated part is running load assessments, where the code automatically generates all input files, but the actual simulations are carried out externally. An overview of the workflow is shown in Figure 4.1. This report studies the design sensitivity

of a single floater concept. The automated design framework initializes by selecting an initial concept, in the present case this is the UMaine VolturnUS semisubmersible floater. The floater design has been parameterized to enable automatic generation of floater geometry descriptions using the design variables as inputs. For the base case, the design variables are defined as the outer diameter of the tower base column, the outer diameter of the buoyancy column, the floater radius, and draft and mooring line length. This selection of design variables is based on a compromise between including the most possible variables of interest and keeping the computational expenses reasonable. The work presented in Section 4 includes work from the related publication (Yildirim et al., 2024).

Studying the design sensitivity requires introducing design variations organized in a Design of Experiment (DOE). A DOE choice suitable for the present problem is the Central Composite Design (CCD) - with five dimensions corresponding to the five design variables of interest. The boundaries of the CCD are constrained based on the condition that all design points in the CCD should result in valid design configurations. Based on this condition, the design interval is defined iteratively until all constraints are satisfied. After selecting the design intervals and design points within them, the designs and their associated limit states are evaluated both in frequency domain and in time domain. The methodology applied is discussed below in details.

Time domain simulations could be beneficial for capturing the nonlinearities in a FWT system, especially for ULS where the maximum motions or forces are required. A comparison of time domain and frequency domain optimization of mooring lines of a FWT considering material cost and cumulative fatigue damage is investigated by (Pillai et al., 2018). Both optimization processes yield aligned designs, however the frequency domain optimization (computing FLS) results in an underprediction of the fatigue loads and misinterpretation of the FLS condition for the frequency domain model implemented. ULS and FLS are also compared using the tools FAST and QuLAF (in the time and frequency domains respectively) to investigate the model performance of QuLAF (Madsen et al., 2019). The ULS results showed that there is under-prediction of the nacelle acceleration due to over-damping of the tower vibrations and overprediction of tower base moments at stronger wind speeds (Madsen et al., 2019). The model provides accurate results for heave, pitch motions, and tower base moments. For FLS the model shows good agreement at the tower base DELs (Pegalajar-Jurado et al., 2018; Madsen et al., 2019) which makes QuLAF suitable for the preliminary design exploration for at least a part of the relevant limit states.

A global sensitivity analysis for a 4-column semi-submersible design is performed in Zhou et al. (2021), which concludes that column radius has the highest effect on the overall design cost and specifically on the surge natural frequency, whereas pitch and tower fore-aft natural frequency were highly dependent on column spacing. Additionally, the factors with the most influence on surge, pitch, and tower top acceleration in waves were identified as column spacing, column radius, and the platform draft.

4.1 Definition of design space: Central Composite Design

We implement a statistical experimental design named CCD which combines factorial and fractional designs. The CCD is particularly applicable to fit low-order polynomial regression models and response surfaces (Ait-Amir et al., 2015). Three main types of CCD configurations depending on the location of the design points are available for consideration, namely circumscribed, face-centered, and inscribed designs. For the circumscribed and face-centered designs, the shape of the pattern means some design points may fall outside of the design boundaries which are

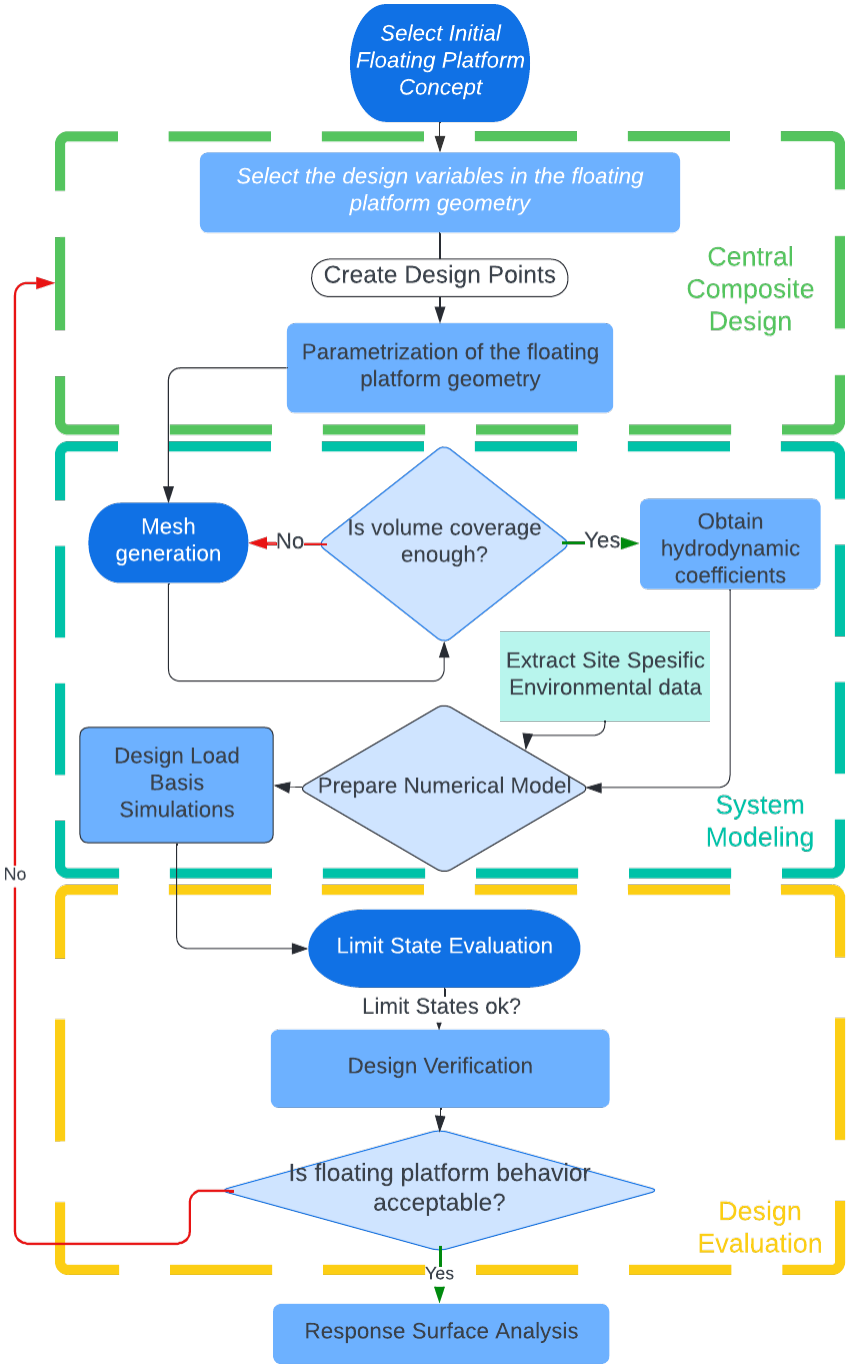

Figure 4.1: Flowchart for the applied methodology

rectilinear and normally defined for one variable at a time. In this report we use an inscribed CCD as a DOE, thus avoiding the issue of exceeding design boundaries (Ait-Amir et al., 2015).

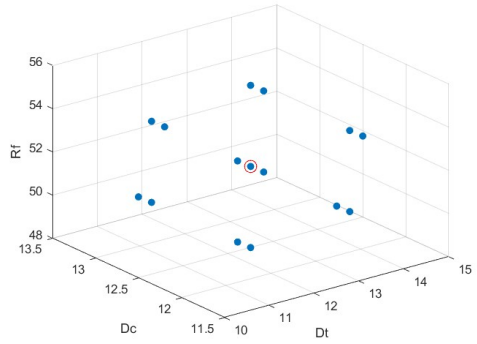

Figure 4.2: Design experiment defined for the sensitivity analysis (Yildirim et al., 2024)

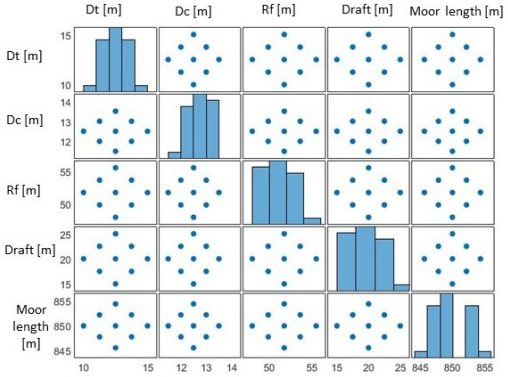

Figure 4.3: Pairplots of the variables in the design space (Yildirim et al., 2024)

The shape of the DOE is illustrated in 4.2 with three of the five variables: floater radius (Rf), buoyancy column diameter (Dc), and tower base diameter (Dt). The full combination of design points and the dimensions of the space are introduced as pair plots in Figure 4.3. This study aims to conduct a sensitivity analysis and not to design a new floater. The red marker in the center of Figure 4.2 is the UMaine semisubmersible design, which is assumed as a baseline and as being the "most feasible" for the sensitivity study, and therefore it is placed as a central point in the DOE.

4.2 Parameterization of floater dimensions and Mesh Generation

The floater surface needs to be meshed in order to make a numerical computation of its hydrodynamic properties. In our framework, the mesh is created using *pygmsh*, which is the Python interface for the 3-D finite element mesh generator *gmsh* (Geuzaine and Remacle, 2009). Once the floater geometry is parameterized through the selected design variables, the mesh for each design point is created automatically. Unstructured mesh is used for 2-D surface mesh generation, and only the submerged part of the floater is meshed. The mesh of the submerged part of the floater and the design variables are illustrated in 4.4. The draft shown is the vertical distance from the bottom of the floater to the free water surface, while the plotted mooring line is only showing its top part. The values for the reference design variables are listed in Table 4.1.

Table 4.1: Design Variables of the floater dimensions in the base case

Design Variables	Description	Reference Design Values
D_t	Outer diameter of tower base column	10 m
D_c	Outer diameter of buoyancy column	12.5 m
R_f	Distance of buoyancy columns from center	51.75 m
L_d	Draft	20 m
L_m	Mooring Line length	850 m

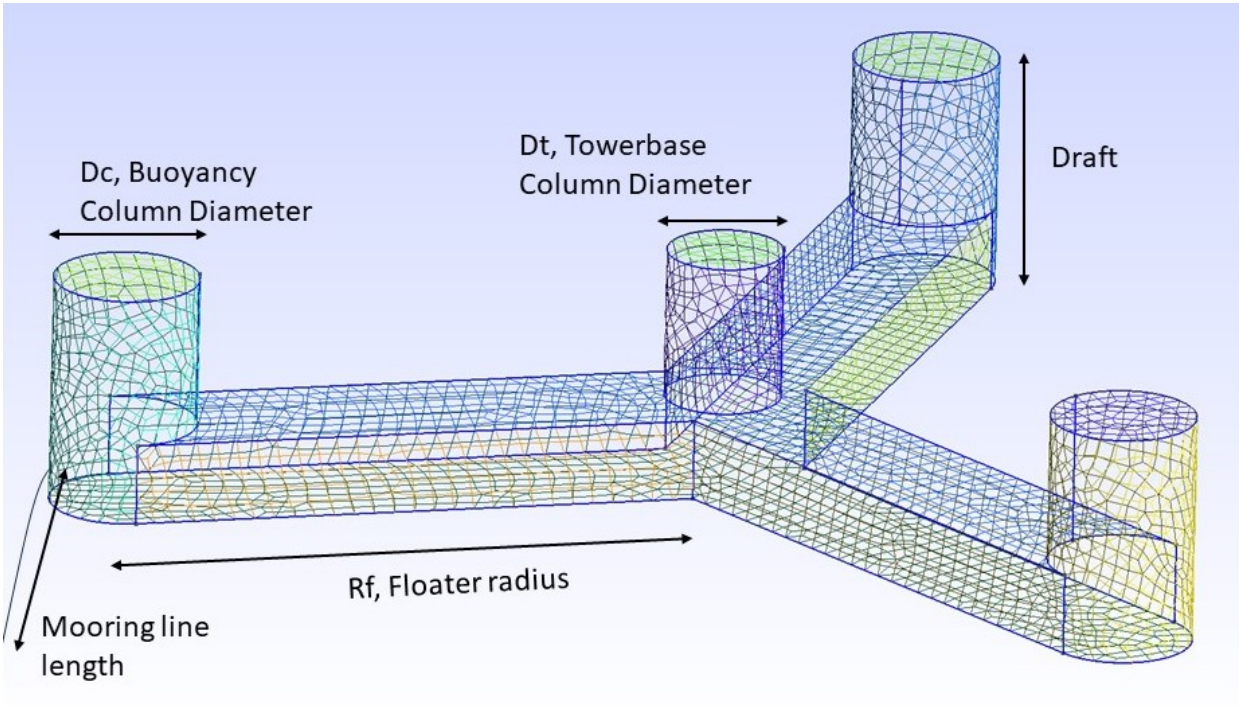

Figure 4.4: Selected design variables for the floater parametrization (Yildirim et al., 2024)

To have consistency for different design points, a mesh sensitivity analysis is conducted initially, and limits for maximum mesh size are defined to ensure accuracy and computational efficiency. The maximum mesh element size is defined as 2 m. This is performed based on a comparison of the submerged volume of the floater and the volume of the mesh generated. Parameterizing floater geometry and automating mesh generation ensures the ability to implement other floater types efficiently. For instance, increasing the number of buoyancy columns or optimizing the components with sections with different diameters.

4.3 Computation of hydrodynamic coefficients

Hydrodynamic coefficients are obtained using the surface mesh generated in the previous step and the open-source panel code (potential flow solver) HAMS/pyHAMS (Liu, 2019). The potential flow approach is a widely used method in offshore/marine engineering for hydrodynamic problems. This method is applicable with the assumption of irrotational flow where viscous effects are neglected. Potential flow theory is the preferred way for obtaining hydrodynamic coefficients that feed the HAWC2 aeroelastic model for the limit state computations. As mentioned above, the hydrodynamic coefficients computation is carried out with the open-source boundary element method software, HAMS (Liu, 2019). A comparison of HAMS with another popular tool for hydrodynamic computations, WAMIT, is shown in Figure 4.5 and Figure 4.6. Added mass, radiation damping, and wave excitation force coefficients are computed in the frequency domain. Since the viscous effects are disregarded within the potential flow approach, additional damping computed as in Kim et al. (2022) for the Hiperwind model is added to the system to account for viscosity effects.

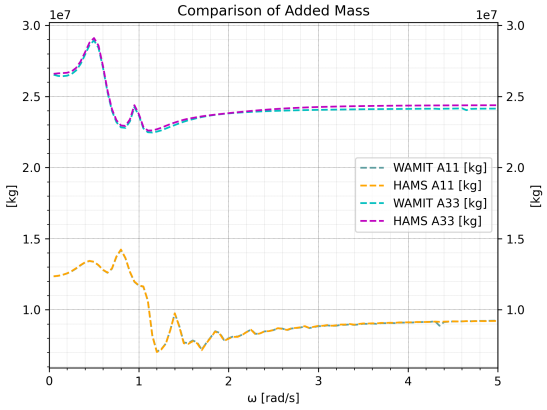

Figure 4.5: Comparison of hydrodynamic coefficients for surge and heave

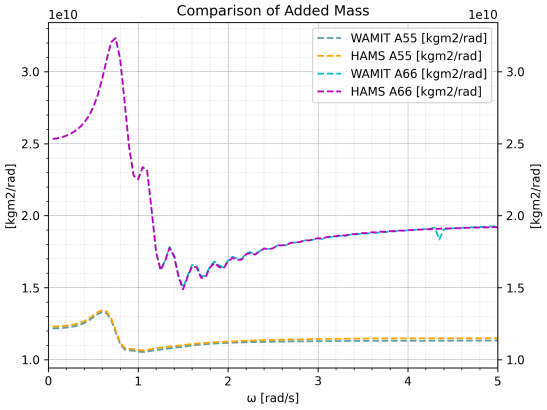

Figure 4.6: Comparison of hydrodynamic coefficients for pitch and yaw

4.4 Wind turbine model preparation

The Hawc2 wind turbine model implementation is based on similar implementations with bottom-fixed versions of the IEA 15MW reference wind turbine. Apart from replacing the fixed support structure with a floater, the other major modification of the model is the change of the controller. An updated version of the controller was needed which includes a feedback signal from tower top motion.

After obtaining the hydrodynamic coefficients, the design evaluation framework automatically generates the files containing the input commands for running HAWC2 simulations. Further, several files used by HAWC2 that define component properties (structural and hydrodynamics) are generated. These include descriptions of tower, floater and mooring lines. The mooring line module of HAWC2 has a dynamic mooring line model (Hansen, 2008) based on non-linear elements where each mooring line element has 6 DoFs (Gözcü et al., 2022). The comparison of dynamic and quasi-static mooring line models on the Hywind Spar indicates that the extreme and fatigue loads on the blades are not affected by the selection of mooring line model (Kallesøe and Hansen, 2011). The dynamic mooring model for the computation of the tower base bending lifetime DEL resulted in a reduction of 5-10 % which ensures cost reduction on the system (Kallesøe and Hansen, 2011).

4.5 System Response

System responses are computed with two different approaches: in time and frequency domains respectively. The primary approach is the time-domain simulations with a fully coupled nonlinear HAWC2 model, which contains a flexible tower and blades, utilizes a potential flow solution for the hydrodynamic loads, and a dynamic mooring line model. A set of Design Load Basis (DLB) simulations with the time domain approach are carried out at each point in the design evaluation DOE. The second approach includes obtaining system responses with the linear frequency-domain model "Quick Load Analysis of Floating Wind Turbines" (QuLAF) developed by DTU (Pegalajar-Jurado et al., 2018). The model considers 4 DOFs including surge, pitch, heave, and first tower modal deflection. Within the model, the wave and wind loads on the structure are precomputed using HAWC2 Larsen and Hansen (2007) and WAMIT (Pegalajar-Jurado et al., 2018) to increase the accuracy and reduce computational needs. The computation uses linearized mooring line

stiffness matrices. Aerodynamic and hydrodynamic loads are assumed independent from each other. More information about the theory and implementation can be found in the literature (Pegalajar-Jurado et al., 2018; Madsen et al., 2019).

Table 4.2: Natural Frequency [Hz] comparison of Umaine floater with IEA 15MW turbine

DOF	Result - QuLAF	Reference (Allen et al., 2020)	Rel.Error
Surge	0.0075	0.007	6.67 %
Heave	0.0598	0.049	18 %
Pitch	0.0352	0.036	-2.17 %
Tower	0.5624	0.5	11.09 %

The natural frequencies are computed using QuLAF and compared to references in literature (which are computed by HAWC2) in Table 4.2. The values for surge and pitch natural frequencies have good agreement with the reference values. The heave natural frequency computed by QuLAF has a larger deviation from the reference value compared to other frequencies; this might be caused by the differences in the modeling approach. Although there is a difference in the geometry representations between the tools, the difference is negligible for the submerged volume and mass properties. For the floater mass, the difference is around 0.6 %. To ensure similar mass and volume values in the models, the pontoon diameter and ballast values are adjusted. After model setup and comparison, the design criteria are evaluated using the system responses. The criteria considered for the evaluation are discussed below.

4.5.1 Design Evaluation Constraints

The variable constraints for the design evaluation are defined based on the site-specific data and the limits of stable and efficient operation for the turbine. The constraint values for the initial evaluation are given in Table 4.3. The selected design points are evaluated considering the variable limits for surge, pitch motion, natural frequencies, as well as additional criteria. From the constraints considered, the pitch motion is significant for optimal energy production and system stability, surge displacement is important for locating the turbine and dynamic cable motion/integrity. Pitch and surge motion limits are defined according to the findings in Mahfouz et al. (2020) and Dou et al. (2020). The stability of the floater is also considered during the design evaluation. Natural frequency constraints are implemented considering the wind, wave spectrum, and blade 1P and 3P frequencies (Allen et al., 2020). Although it is a common approach to also consider the 6P frequency, it is omitted here. Also, only a part of the operational load cases are simulated, namely focusing on cases with rated wind speed and the corresponding wave conditions. Since the goal of this study is primarily to establish design sensitivities, it is most important to consider relative differences between design realizations - and a simplified load case setup is deemed sufficient.

4.5.2 Response Surface Analysis

The outcomes of the design response evaluations are used to fit first- and second-order response surfaces. With the CCD as a DOE, a second-order response surface fit is only feasible if all points of the DOE have valid data. To ensure this, the final design boundaries are defined iteratively.

Table 4.3: Constraints used in the design evaluation for the central composite design

Constraint	Description	Value	Unit
1	Maximum Surge Offset	$\lvert\xi_{surge}\rvert < 30$	m
2	Maximum Pitch Angle	$\lvert\xi_{pitch}\rvert < 10$	deg
3	Surge Natural Frequency	$f_{n,surge} < \frac{1}{100}$	Hz
4	Pitch Natural Frequency	$\frac{1}{35} < f_{n,pitch} < \frac{1}{25}$	Hz
5	Tower Natural Frequency	$f_{n,tower} > 0.439$	Hz

Each step in the iterative process includes running simulations at the design points using QuLAF and HAWC2 and evaluating the design constraints. If the predefined limits are violated for a given design point, the design space is narrowed down in the given dimension, and the affected design points are re-evaluated in a following step. Once the final design space has been established, linear and quadratic polynomials are fitted to the maximum values of surge offset and pitch motion, and to the natural frequencies. The resulting polynomials generate the response surfaces which now provide continuous mapping between design variables and the expected response. Such continuous mapping is necessary for the design sensitivity analysis discussed below, as variance-based sensitivity analysis normally requires a large number of function evaluations which are not easily obtainable with the high-fidelity models. The present methodology was chosen due to its relative simplicity and the small number of design point evaluations required to fit the response surface. One of its potential limitations is that the Central Composite Design allows fitting a polynomial of at most second degree, meaning that the model may perform poorly in predicting highly nonlinear responses (Dimitrov et al., 2018). For future studies, further validation of the response surface methodology with different fits and experimental designs should be investigated.

Another limitation of the investigations in this work is the small design space for the floater. This can not be avoided with the current methodology due to the design evaluation constraints. One improvement to prevent this issue can be the introduction of a preliminary optimization scheme for the mooring lines. In this study, the approach is to check mooring line design and only mooring length is considered as a design variable without modifying the chain diameter.

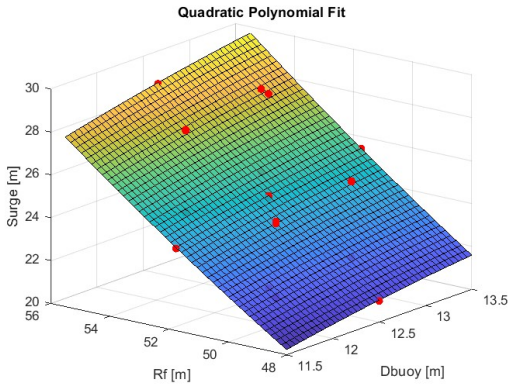

Figure 4.7: Quadratic polynomial fit to the surge response (Yildirim et al., 2024)

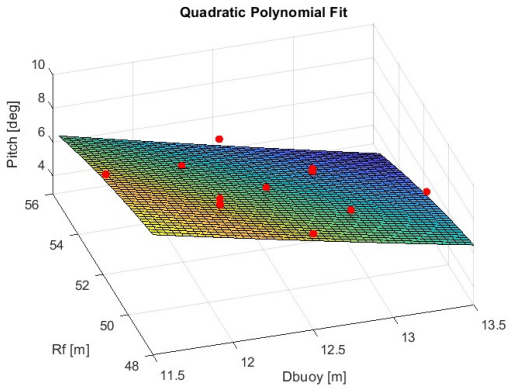

Figure 4.8: Quadratic polynomial fit to the pitch response (Yildirim et al., 2024)

125 different response surfaces are generated by choosing different combinations of input

variables, different polynomial order (first or second), and using data from different tools (QuLAF and HAWC2). The coefficient of determination (R-squared) is evaluated as a goodness of fit criterion. The R-squared is a measure of the proportion of the variance of the dependent variable that is predictable from the independent variables.

The response surfaces generated using a quadratic fit on FWT surge and pitch responses from QuLAF outputs are shown in Figure 4.7 and Figure 4.8 respectively. The input variables on the x- and y-axis are floater radius (R_f) and buoyancy column diameter (D_{buoy}). In the figures, the red points on the response surface present the selected designs.

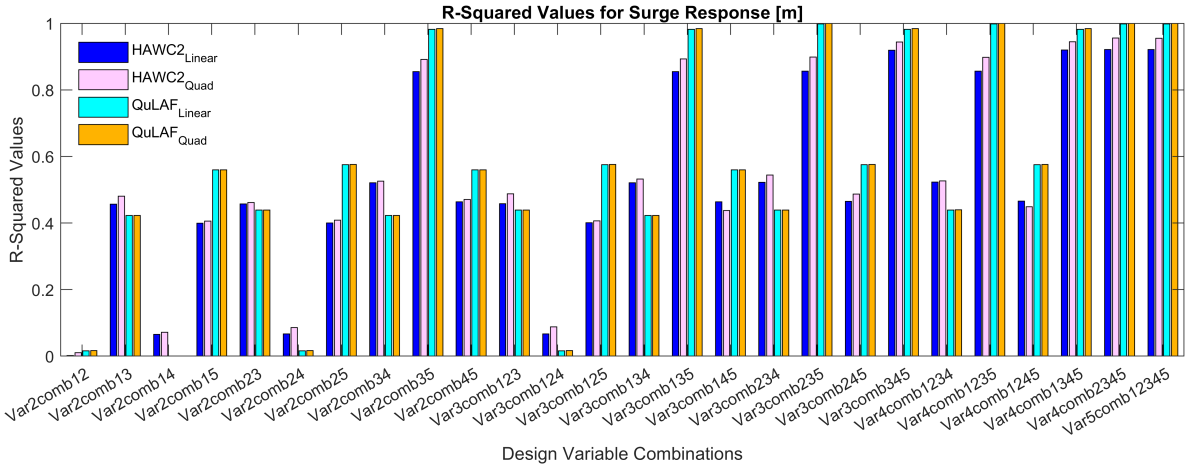

Figure 4.9: R-squared for the quadratic fit to the surge response (Yildirim et al., 2024)

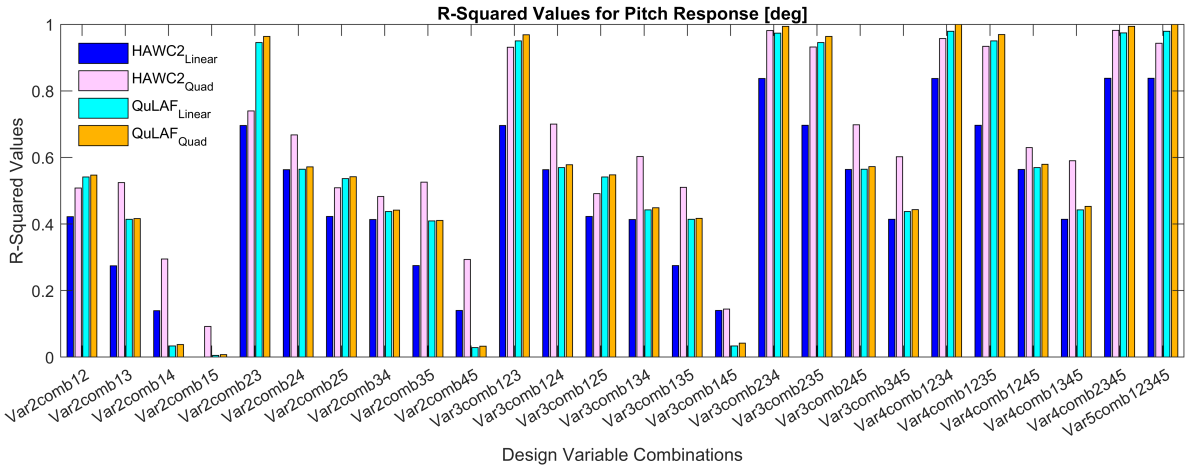

Figure 4.10: R-squared for the quadratic fit to the pitch response (Yildirim et al., 2024)

The R-squared values for quadratic and linear fits of surge and pitch responses are shown in Figures 4.9 and 4.10. In these plots, the x-axis presents different combinations of design variables. This presentation helps identify variables and their combinations that have high impact on the FWT response. The considered design variables and related numbering in the Figures are given as: Variable 1 is the tower base diameter, variable 2 is the buoyancy column diameter, variable 3 is the floater radius, variable 4 is the draft, and variable 5 is the mooring line length. For instance, in Figure 4.9, "var3comb135" means that three design variables - variable 1 (tower base diameter), variable 3 (floater radius), and variable 5 (mooring line length) are used to generate the response

surface for Surge offset and its R-squared value is computed for that fit and presented in the Figure 4.9.

The R-squared values that are compared for the linear and quadratic polynomial fits for the frequency domain (QuLAF) outputs present almost identical performance. When the same comparison is carried out for data obtained from time-domain HAWC2 simulations, the differences between the linear and quadratic fits are larger. For the HAWC2 responses, quadratic fits perform better. The difference is visible especially for the pitch response, suggesting this response variable is most affected by non-linearities in the FWT system. Additionally, the differences in the control approaches implemented in QuLAF and HAWC2 models might also contribute to the observed discrepancy. Despite that the quadratic fit is better at predicting the response of the HAWC2 model, still the R-squared values are lower than those for the QuLAF response surface fits. This is a further indication that the HAWC2 response is affected by nonlinearities which may require higher than second-order surface in order to predict with high precision. Figure 4.9 shows that when the design variables floater radius and mooring line length (variable 3 and variable 5) are used, higher R-squared values are obtained for the surge motion. Buoyancy column diameter has a higher effect on all sets of response in Figure 4.10 and Figure 4.11.

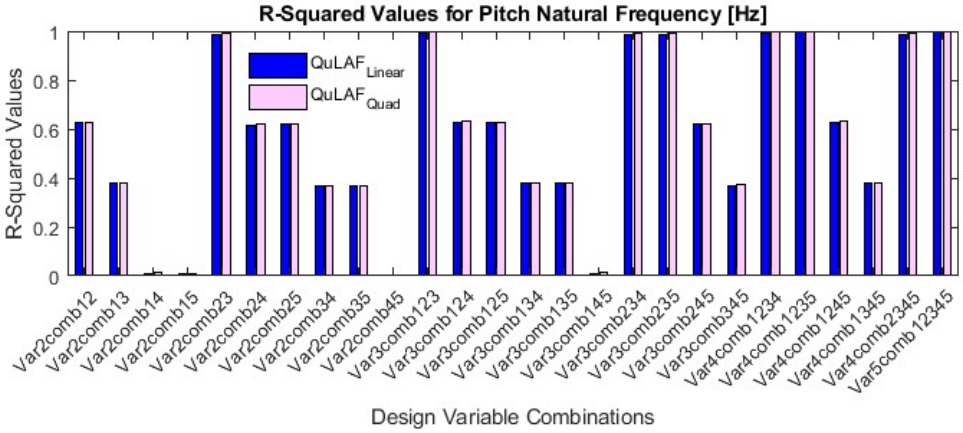

Figure 4.11: R-squared for the quadratic fit to the pitch natural frequency (QuLAF results) (Yildirim et al., 2024)

There is no explicit representation of the rotor and blade position in QuLAF; therefore, the blade-water clearance is only available for the HAWC2 model output. For the blade-water clearance, the quadratic polynomial fit provides a better approximation compared to the linear response surface fit. Figure 4.12 presents the comparison of fits for HAWC2 outputs and it demonstrates that the draft has higher significance in terms of blade-water clearance and has higher contribution to R-squared values.

4.6 Global variance-based sensitivity analysis

The previous section presented a qualitative comparison of the effect of different design variables on the system response. As a next step, we will compute a quantitative estimate of this dependence using variance-based sensitivity analysis. The Sobol indices (Sudret, 2008) provide an estimation of the individual, relative contribution of each input variable to the variance of the output (hence the term variance-based sensitivity analysis). The Sobol indices are computed with the help of a Polynomial Chaos Expansion (PCE), which is a regression model based on orthogonal

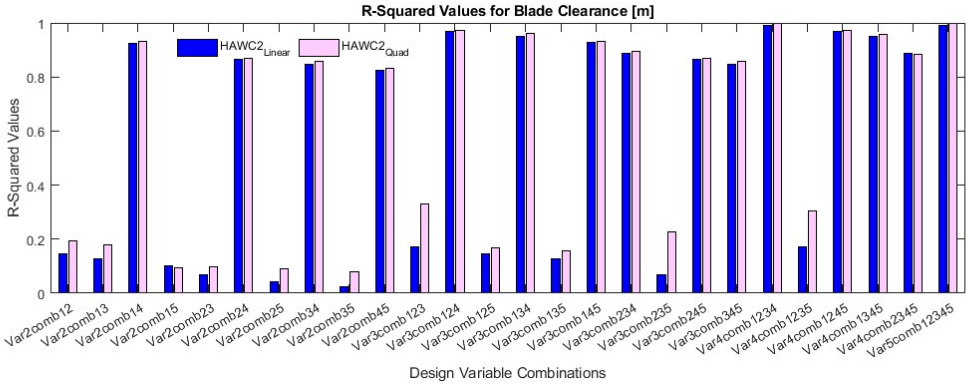

Figure 4.12: R-squared for the quadratic fit to the blade clearance (Yildirim et al., 2024)

polynomial terms (Sudret, 2008). The orthogonality property means the individual contribution of each polynomial term to the output variance can be analytically determined, and then Sobol indices for each input variable are obtained by summing the contributions from polynomial terms where the variable is present. The UQLab tool (Marelli and Sudret, 2014) is used to train a PCE model and compute first-order and total-order Sobol Indices using the same datasets generated for the response surface fits presented earlier.

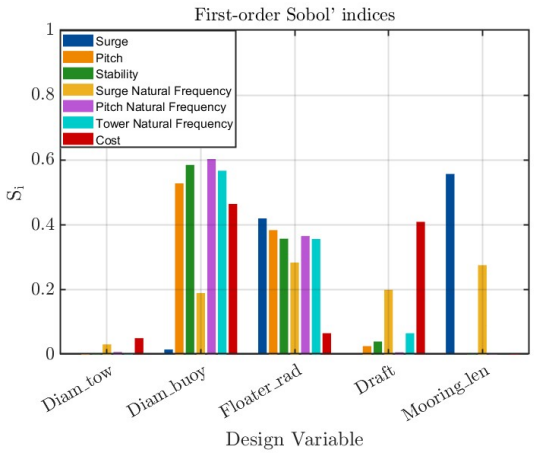

Figure 4.13: QuLAF first order Sobol Indices (Yildirim et al., 2024)

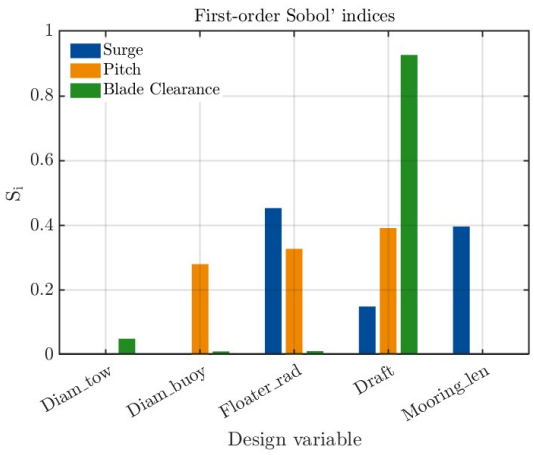

Figure 4.14: HAWC2 first order Sobol Indices (Yildirim et al., 2024)

The outputs of the global sensitivity analysis of the design variables defined in Table 4.1 on the system response computations performed with QuLAF are given in Figure 4.13. The comparison highlights that the buoyancy column diameter has the most significant effect on the system response. Changing the buoyancy column diameter affects almost all system responses. Further, surge response and natural frequency are affected by multiple variables. Buoyancy column diameter has the highest Total Sobol Indices, followed by floater radius, mooring line length, and draft. Mooring line length has a relatively small impact. The relatively narrow design space for the mooring line length can be the reason. Comparing the time and frequency domains, there are large differences in the QuLAF and HAWC2 Sobol indices (see Figure 4.13 and Figure 4.14). For buoyancy column diameter and pitch, the large difference of Sobol indices indicates system physics which may not be fully captured by one of the models. As shown in Figure 4.14, the

first-order Sobol Indices are slightly higher for the draft on the surge and pitch motion in HAWC compared to QuLAF. The difference in the modeling includes different seeds used for the loads, using an active controller in HAWC2 and non-linearities due to large rotations.

4.7 Conclusion

This section presented a framework for floating wind turbine design assessment, to evaluate the effect of floater design modifications on the structural limit states. Using response surface fits to model realizations generated with time domain and frequency domain tools, a variance-based sensitivity analysis is performed on the Umaine Semisubmersible floater design. The outcome of the analysis reveals that the buoyancy column diameter and floater radius have the higher influence on the design response among the variables investigated.

5 Serviceability Limit State assessment

5.1 Overview of SLS modes relevant for FOWT

Structural design requires the definition of relevant strength limit states to ensure that the design integrity is maintained during the operational life of the structure. In addition to load resistance, safe operation within functional performance limits and behavior preserving the economic gain are also required. Serviceability limit states (SLS) cover this aspect. SLS can be classified into three main categories: deformation including local damage to nonstructural elements, motion perception in terms of excessive vibration and acceleration, and finally, deterioration of components due to corrosion, fatigue, and weathering (Griffis, 1993). As mentioned in Section 2.3, the serviceability limit states for FWTs are not well defined in the current standards, and they are subject to the designer and operator's choices.

According to (GL, 2018), SLS relevant for FWTs can be deformations affecting the efficiency of the components or operation of the turbine, cracks affecting the water tightness, excessive motion which affects the structural components, corrosion reducing structural durability, and anchor resistance for grouted rock anchors. According to the same reference, Accidental Limit States (ALS) with high economic or social losses or with an annual probability of occurrence less than 10E-3 should also be treated as SLS. Hence, as discussed in Section 2.3, ship collision to a FWT system may cause severe losses and it should be considered as SLS. In addition to the limiting value for a single FWT as deformation of rotor blades and tower inclination, farm-level limits should also be considered to restrict FWT motion to prevent damage on subsea cables or neighboring facilities (IEC, 2019).

In addition to the concept classification, FWT systems can be grouped into two categories with respect to materials: steel and concrete floaters. Concrete floaters have been an alternative to steel floaters due to reduced material cost, better logistics, and manufacturing availability. Concrete floaters require additional SLS to ensure safe operation due to the specific material properties. According to (ABS, 2015), additional requirements are limiting the reinforcing stress and limiting membrane strain in hollow cross sections, to avoid appearance of cracks. The criteria are dependent on the amount of pre-stressing applied to the structure, and are evaluated under a worst-case loads combination, however witout application of safety factors.

Additional SLS criteria for the FWT systems can be defined based on the limitations during

the installation process including the motion limit of the structure for safe towing, floatability for reducing the transport costs, and for simpler transportation. Farm-level SLS which limits floater motion for safe farm operation can be also important for FWT systems. Farm-level SLS can be defined based on the wind farm layout, turbine placement, dynamic cable properties, and orientation. Anchor position can also be considered as an SLS for FWT systems. The effect of the position of the anchors (installation error) or change in soil stiffness within time can be considered.

5.2 Limit state computation

SLS computation for the reference design is performed using 10185 HAWC2 simulations for the reference design case with nominal floater dimensions. Six wind and three wave seeds are used for each combination of environmental conditions. The comparisons are performed for the HAWC2 outputs of rotor thrust, tower base fore-aft and side side moments, platform motions in six degrees of freedom, mooring line tensions, blade clearance to tower and water, tower top motions, and accelerations. The results of the SLS computations are shown in the following section, along with FLS and ULS.

6 Case Demonstration at the South Brittany Site

This section demonstrates global limit state (ULS, FLS and SLS) computation for the reference floater design at the South Brittany site. Only time-domain simulations are performed using HAWC2. The input files for the HAWC2 simulations are prepared as discussed in Section 4. The simulations are performed on the Sophia HPC Cluster at the Technical University of Denmark. The dynamic responses are modelled under operational, non-operational, and fault conditions as prescribed by the DLCs (Design Load Cases) in IEC61400-3 (IEC, 2019). The DLCs modeled in this study are presented in Table 6.1. The site parameters are extracted from the distributions defined in Section 3.3. For the specific load cases (for example DLC 1.6) an environmental contour approach is implemented to obtain combinations of site parameters coming from joint distributions such as wind speed, wave height, and peak period.

Simulation length is determined based on the selected DLCs and the first 200 seconds are discarded during the post-processing. The length of the simulations is defined based on the recommended duration per DLC as prescribed in the IEC guideline (IEC, 2019). In addition, the first 200s are discarded from each simulation to remove the initialization phase of each simulation. This initial transient time is assumed longer for FWTs compared to the onshore turbines due to the complexity of the system and the low natural frequency of some of its components. The Jonswap spectrum is used to generate irregular waves, and turbulence realizations are generated according to the Mann spectrum with a turbulence generator integrated within HAWC2.

6.1 Postprocessing of simulation results

The time series outputs from the HAWC2 simulations of the FWT model have been refined by selecting the important output channels to reduce the computational time. The channels for data processing are defined based on the relevancy for evaluating the SLS (and other limit states) of the FWT system. During the post-processing, statistical descriptors of the data are extracted, and damage equivalent loads (DELs) are computed for the tower base and mooring lines. DELs

Table 6.1: DLCs considered in this report

Name	Limit State	Description	Name	Limit State	Description
DLC 1.1	ULS	Normal production	DLC 3.3	ULS	Start-up
DLC 1.2	FLS	Normal production	DLC 4.1	FLS	Shut-down
DLC 1.3	ULS	Normal production	DLC 4.2	ULS	Shut-down
DLC 1.4	ULS	ECD	DLC 5.1	ULS	Shut-down
DLC 1.5	ULS	EWS	DLC 6.1	ULS	Parked
DLC 1.6	ULS	Normal production	DLC 6.2	ULS	Parked
DLC 2.1	ULS	Grid Loss	DLC 6.3	ULS	Parked
DLC 2.2	ULS	Error (pitch runaway, extreme yaw error, one blade stuck)	DLC 6.4	FLS	Parked
DLC 2.3	ULS	Grid Loss	DLC 7.1	ULS	Rotor locked and Extreme yaw
DLC 3.1	FLS	Start-up	DLC 7.2	FLS	Rotor locked and normal wind
DLC 3.2	ULS	Start-up	DLC 8.1	ULS	Maintenance

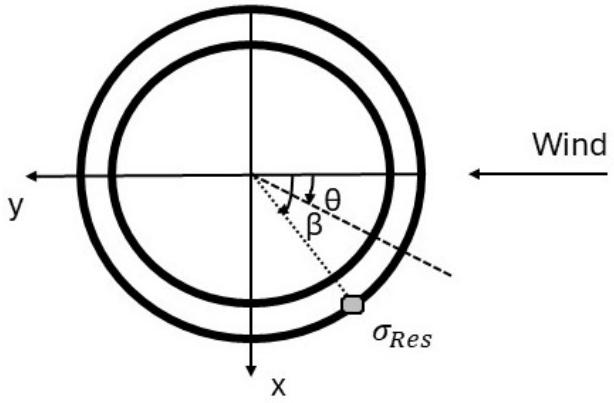

Figure 6.1: Coordinate system for the computation of tower base stresses

are calculated based on the Palmgren Miner rule. The equation for the computation of DELs is given below:

$$S_{eq} = \left[\frac{\sum_{i=1}^{K} n_i S_i^m}{n_{eq}} \right]^{\frac{1}{m}} \tag{6.1}$$

where the S_i is the load/stress amplitude of a number of cycles n_i in the i^{th} bin, and m is the Wöhler exponent. n_{eq} is the number of equivalent cycles over a reference period, i.e., in order to compute a 1Hz-equivalent DEL over a 10-minute period, n_{eq} should equal 600. K is the total number of bins for DEL computation.

6.1.1 Computation of Tower base Stresses

As a post-processing step, the tower base axial stress (Equation 6.2) is computed at the outermost location of the tower measured from its center based on the global coordinate system of HAWC2. The coordinate system used in Equation 6.2 can be seen in Figure 6.1 where β is the angular location on the tower base where stresses are being computed, and θ is the wind direction. $\sigma_{Res}(\beta)$ is the resultant tower base stress computed at azimuth location β around the tower.

In Equation 6.2, σ_{Res} is the axial stress in gravity direction (+z-direction), A is the cross-sectional area of the tower base with cross section thickness t, M_x and M_y are bending moments at the tower base in the global coordinate system. I_x and I_y are the area moments of inertia of the cross-section in the x and y directions respectively.

$$\sigma_{Res}(\beta) = \frac{F_z}{A} + \frac{M_x}{I_x} r\cos(\beta - \theta) + \frac{M_y}{I_y} r\sin(\beta - \theta) \tag{6.2}$$

A stress concentration factor (SCF) is applied to the resultant nominal stress at the tower base. The SCF values are defined at each welded section for the modified tower during previous work in the Hiperwind project, following DNV recommendations (Veritas, 2010). The same SCF is used here to compute hot spot stresses at the tower base. The DEL computation discussed in

Section 6.1 is initially performed for each time series. For the DLC simulations, different wind and wave seeds are simulated. To evaluate the FLS, the computed DEL values are averaged within the wind/wave seeds, and lifetime DELs are computed using the wind speed and wind direction sector joint probabilities for the South Brittany Site. The wind rose for the site can be found in Figure 6.5. The $DEL_{lifetime}$ values are computed using the formula below:

$$DEL_{lifetime} = \left[\frac{\sum_{j=1}^{M} p_j \frac{\sum_{i=1}^{N} S_i^m}{N}}{M} \right]^{(1/m)} \tag{6.3}$$

where p_j is the joint probability of wind speed and its direction computed from the 30-year ANEMOC database, and N is the number of seeds for each wind speed including wave seeds. For the DLC 1.2 used in this computation, there were 6 wind seeds and 3 wave seeds for each wind speed. m is the Wohler exponent discussed above and it is defined as $m = 3$. S_i^m is the stress amplitude computed for each time series and M is the number of wind direction sectors multiplied by the number of wind speed bins considered in this analysis. For the computation of DLC 1.2, initially, the simulations are performed for 0-degree wind only. To compute the effect of the different wind directions, the stress field computed is rotated around the tower axis to account for the effect of the wind direction on the tower and finally, the results are superimposed. Figure 6.2 presents the DEL field around the tower cross section computed for 0-degree wind only; and Figure 6.3 presents the time series of the computed values using Equation 6.2. In Figure 6.2 and Figure 6.2, the label "Sigma_120_0" represents the stress value computed for 120 degrees on the tower base due to wind from 0 degrees. Considering the sign convention in Figure 6.1, for "Sigma_120_0", β is 120 degrees and θ is 0 degrees.

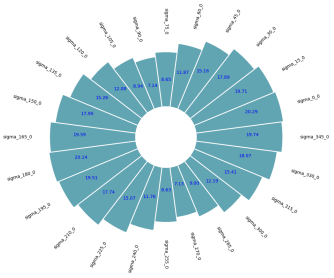

Figure 6.2: Damage equivalent loads [MPa] on the tower base for 0 degree wind direction

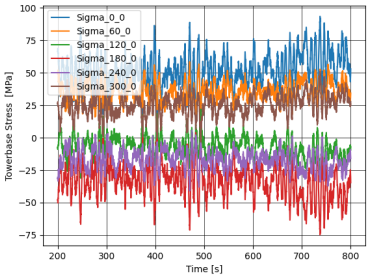

Figure 6.3: Time series of the computed tower base stresses

6.2 DLB Results: FLS and ULS

Tower base ULS and FLS Figure 6.4 shows the lifetime-equivalent DEL distribution over the tower base cross section, computed with the procedure discussed in the previous section. The $DEL_{lifetime}$ distribution follows a fairly uniform pattern. This can be due to the scattered wind rose of the selected site, combined with the symmetry of the bending stresses where applying a bending moment results in high stresses with opposite sign in two diametrically opposite sides of

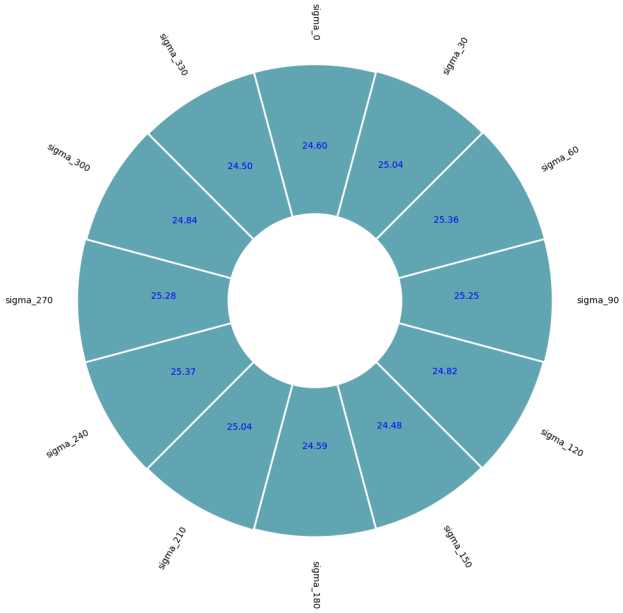

Figure 6.4: Lifetime damage equivalent loads [MPa] on the tower base (DLC 1.2)

the section. For this site, the effect of wind speed distribution is not very significant. In other sites, environmental condition distributions can have a significant effect on the fatigue life of the structure, and by reducing the uncertainties on the wind/direction distribution by selecting more advanced modeling strategies and measurement campaigns, a more efficient design could be possible.

In this report, FLS for the tower base was computed from DLC 1.2 with no wind-wave misalignment consideration. When wind-wave misalignment occurs in the direction perpendicular to wind speed, smaller aerodynamic damping is present in the cross-wind direction which affects the fatigue loads on the structure (Van Vledder, 2013). Therefore, the structure is exposed to larger loads/motion and this should be taken into account in the further detailed design by considering the occurrence probability and magnitude of the wind wave misalignment (Van Vledder, 2013).

ULS and FLS for the station-keeping system According to DNV (2021) the ULS criterion for the mooring lines requires that each mooring line in the station-keeping system should withstand extreme loads with a 50-year return period. ALS for the mooring lines represents the condition where during the failure of one mooring line, the system should be able to survive. FLS criteria require that the mooring lines have the required fatigue strength for cyclic loading. Therefore, in addition to the tower base stresses, the maximum loads on the station-keeping system should be investigated to ensure the ULS criteria for the mooring lines.

6.3 SLS evaluation

Blade clearance to the water surface (minimum distance between blade tip and water surface) is considered an indicator for the SLS assessment of FWTs. According to the results of the simulations performed, DLC 1.6 was found as the most critical DLC for blade tip-water clearance where the minimum distance observed was 29 m from MSL. The blade tip-water clearance values

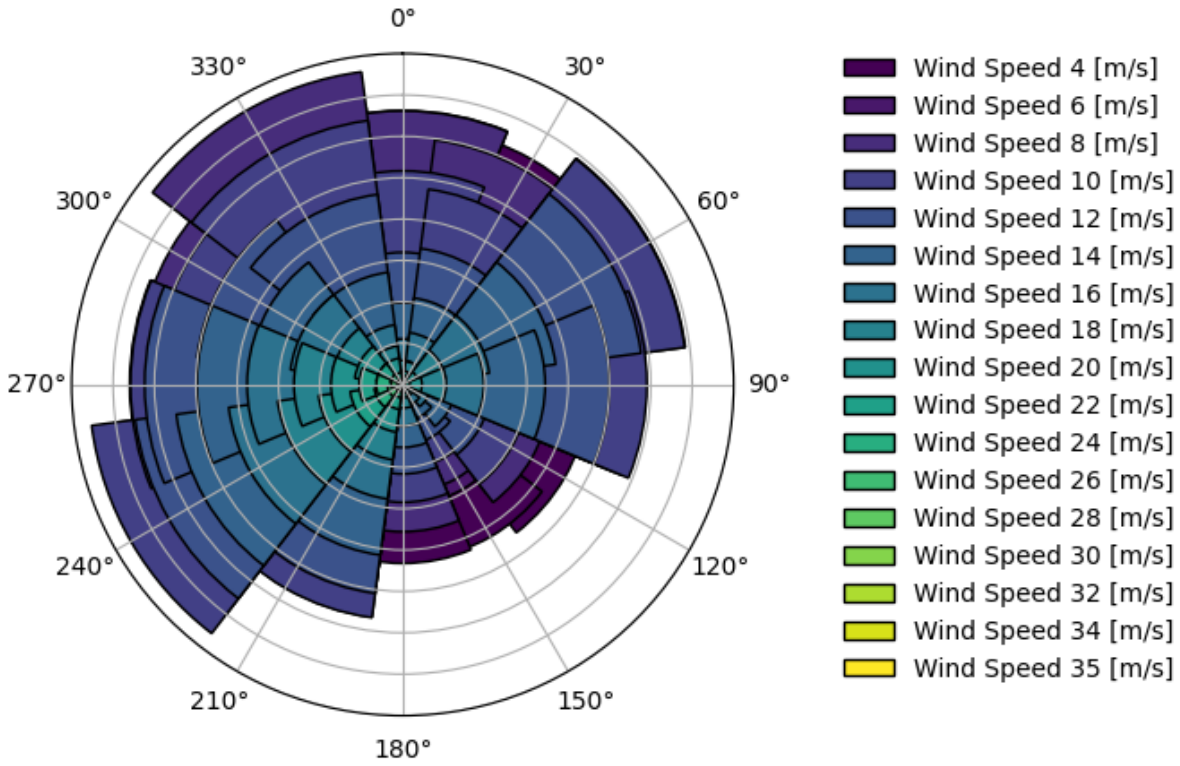

Figure 6.5: Wind rose plot for the South Brittany Site

for different wind speeds in DLC 1.6 can be seen in Figure 6.6. In the figure the values are presented as negative however, this is due to the sign convention of the model used. The value for the minimum allowed blade tip-water clearance SLS depends on the location of the offshore wind farm and local regulations, where marine spatial planning might have a significant influence in defining this limit.

Another serviceability limit state discussed in this work is the blade tip-tower clearance. Blade tip-tower clearance is important in terms of the operational safety of the turbine and for this SLS, the most critical DLC is identified as DLC 1.3, power production during extreme turbulence. The results for DLC 1.3 are presented in Figure 6.7 and as expected lowest clearance values occur at wind speeds associated with the highest thrust forces. For tower top accelerations during operation, the most critical operational case is again DLC1.3, as well as DLC2.1 which represents operation under faulty conditions with grid loss. The results for DLC 1.3 are given in Figure 6.8 and Figure 6.9 for fore-aft and side-side directions respectively, while the same result types for DLC 2.1 are given in Figure 6.10 and Figure 6.11 respectively. From the figures discussed above, we see that the highest fore-aft and side-side accelerations happen when the turbine is parked without a grid connection in a 50-year extreme event. In the absence of aerodynamic damping from the operational turbine, the wave effects cause greater motion of the FWT system.

7 Conclusions

This report presented a semi-automatic, Python-based computation framework for evaluation of the design of Floating Wind Turbine systems. The framework was applied to carry out global

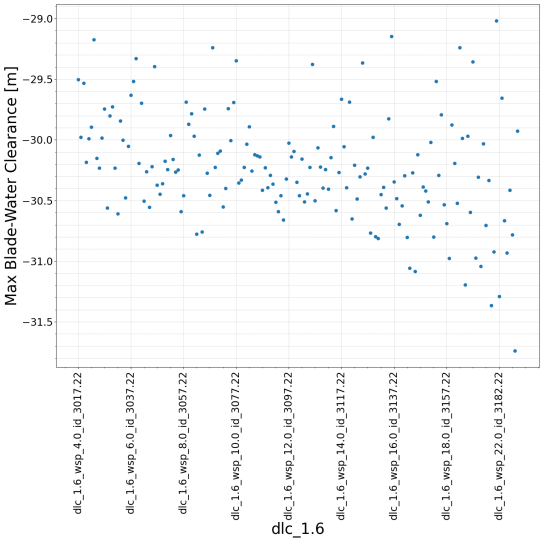

Figure 6.6: Blade water clearance for DLC 1.6

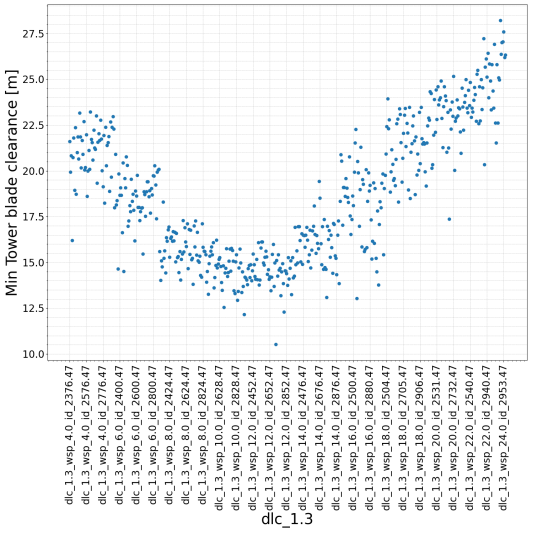

Figure 6.7: Tower blade clearance for DLC 1.3

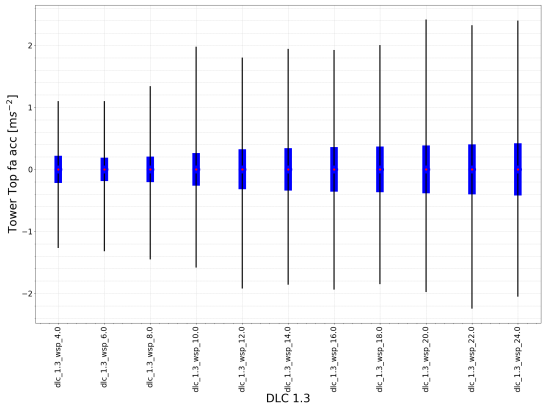

Figure 6.8: Tower top fa acceleration for DLC 1.3

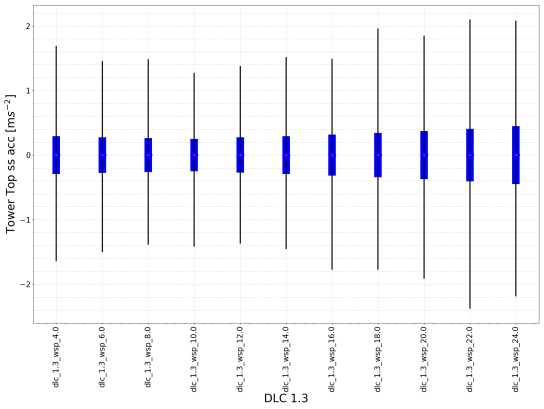

Figure 6.9: Tower top ss acceleration for DLC 1.3

variance-based sensitivity analysis and limit state evaluation for the Umaine semisubmersible floater concept coupled with the IEA 15MW reference wind turbine. Both time- and frequency-domain responses were evaluated, and the floater response sensitivity with respect to five floater design parameters was evaluated: buoyancy column radius, floater radius, tower base column diameter, draft, and mooring line length. The floater response variables considered include: surge, pitch, stability, surge natural frequency, pitch natural frequency, tower natural frequency.

The key findings of the sensitivity analysis are: the buoyancy column diameter has the highest influence on the pitch response, pitch, and tower fore-aft natural frequencies; the change in floater radius also affects the wave response of the structure in the surge, pitch motion, pitch, and tower fore-aft natural frequencies.

Ultimate Limit State (ULS), Fatigue Limit State (FLS), and Serviceability Limit State (SLS) were evaluated, with special focus on the SLS. Blade tip-water surface clearance, blade tip-tower clearance, and tower top fore-aft and side-side accelerations are considered as SLS modes, and the relevant design load cases informative of these SLS are identified. For the blade tip-

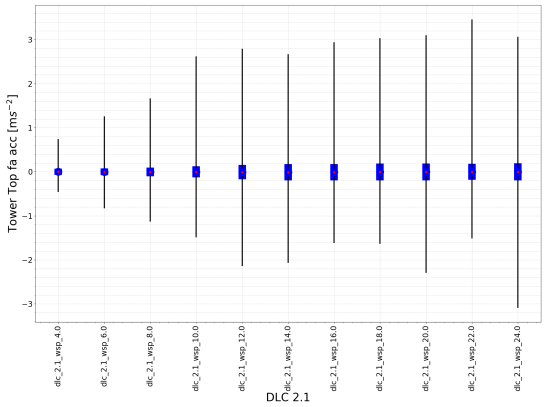

Figure 6.10: Tower top fa acceleration for DLC 2.1

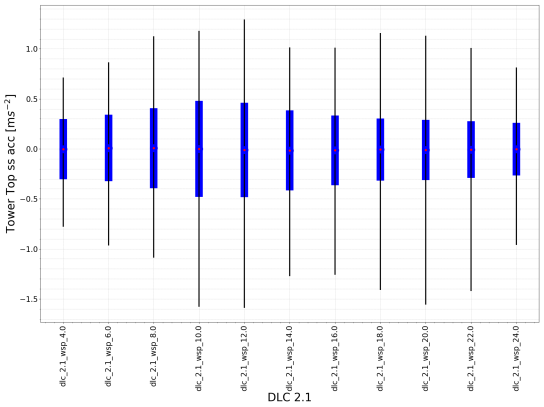

Figure 6.11: Tower top ss acceleration for DLC 2.1

water clearance, the critical load case is identified as DLC 1.6, whereas for the blade tip-tower clearance, DLC 1.3 was critical. Both DLC 1.3 and 2.1 provide the critical values for the tower top acceleration. The DLCs identified in this study can have a dependency on the site conditions and the selected floater configuration. Hence for another floater concept, the identification should be repeated.

The present work lays out the initial steps towards a probabilistic FWT design framework. As one part of such a framework, local and global design sensitivity analysis was performed. The methodology enables the propagation of model input uncertainties, both in the environmental conditions and in the floater properties. Future steps include investigating sampling methods for probabilistic fatigue limit state estimation, methods for faster performance of time-domain simulations (e.g. by using simplified dynamic system representations), and setting up a reliability-based design optimization problem.

Acknowledgements

The work is a part of the HIghly advanced Probabilistic design and Enhanced Reliability methods for the high-value, cost-efficient offshore WIND (HIPERWIND) project, which has received funding from the European Union's Horizon 2020 Research and Innovation Programme under Grant Agreement No. 101006689. The support is greatly appreciated. The authors gratefully acknowledge the computational and data resources provided on the Sophia HPC Cluster at the Technical University of Denmark, DOI: 10.57940/FAFC-6M81.

References

IEC 61400-1: Wind energy generation systems - Part 1: Design requirements. Technical Report, International Electrotechnical Commission, Geneva, Switzerland, 2019.

A. B. o. S. ABS. Guide for building and classing floating offshore wind turbine installations. Technical report, Houston (TX), USA, 2015.

I. B. Ahmad, A. Schnepf, and M. C. Ong. An optimisation methodology for suspended inter-array power cable configurations between two floating offshore wind turbines. *Ocean Engineering*,

278:114406, June 2023. ISSN 00298018. doi: 10.1016/j.oceaneng.2023.114406. URL https://linkinghub.elsevier.com/retrieve/pii/S0029801823007904.

B. Ait-Amir, P. Pougnet, and A. El Hami. Meta-Model Development. In *Embedded Mechatronic Systems 2*, pages 151–179. Elsevier, 2015. ISBN 978-1-78548-014-0. doi: 10.1016/B978-1-78548-014-0.50006-2. URL https://linkinghub.elsevier.com/retrieve/pii/B9781785480140500062.

C. Allen, A. Viscelli, H. Dagher, A. Goupee, E. Gaertner, N. Abbas, M. Hall, and G. Barter. Definition of the UMaine VolturnUS-S Reference Platform Developed for the IEA Wind 15-Megawatt Offshore Reference Wind Turbine. Technical Report NREL/TP–5000-76773, 1660012, MainId:9434, July 2020. URL https://www.osti.gov/servlets/purl/1660012/.

W. Cui, S. Fu, and Z. Hu, editors. *Encyclopedia of Ocean Engineering*. Springer Nature Singapore, Singapore, 2022. ISBN 978-981-10-6945-1 978-981-10-6946-8. doi: 10.1007/978-981-10-6946-8. URL https://link.springer.com/10.1007/978-981-10-6946-8.

N. Dimitrov, M. C. Kelly, A. Vignaroli, and J. Berg. From wind to loads: wind turbine site-specific load estimation with surrogate models trained on high-fidelity load databases. *Wind Energy Science*, 3(2):767–790, 2018. doi: 10.5194/wes-3-767-2018. URL https://wes.copernicus.org/articles/3/767/2018/.

DNV. DNV-OS-E301 Position Mooring, 2021.

G. L. DNV. DNV-OS-J101–Design of offshore wind turbine structures., 2014.

S. Dou, A. Pegalajar-Jurado, S. Wang, H. Bredmose, and M. Stolpe. Optimization of floating wind turbine support structures using frequency-domain analysis and analytical gradients. *Journal of Physics: Conference Series*, 1618(4):042028, Sept. 2020. ISSN 1742-6588, 1742-6596. doi: 10.1088/1742-6596/1618/4/042028. URL https://iopscience.iop.org/article/10.1088/1742-6596/1618/4/042028.

E. Gaertner. Definition of the IEA wind 15-megawatt offshore reference wind turbine. Technical Report TP-5000-75698, NREL, Golden, CO, 2020.

C. Geuzaine and J.-F. Remacle. Gmsh: a three-dimensional Finite element mesh generator with built-in pre- and post-processing facilities. *International Journal for Numerical Methods in Engineering*, 2009. ISSN 00295981.

D. GL. DNVGL-ST-0119: Floating wind turbine structures. Technical report, 2018.

L. G. Griffis. Serviceability Limit States Under Wind Load. *ENGINEERING JOURNAL*, 1(30): 1–16, 1993.

O. Gözcü, S. Kontos, and H. Bredmose. Dynamics of two floating wind turbines with shared anchor and mooring lines. *Journal of Physics: Conference Series*, 2265(4):042026, May 2022. ISSN 1742-6588, 1742-6596. doi: 10.1088/1742-6596/2265/4/042026. URL https://iopscience.iop.org/article/10.1088/1742-6596/2265/4/042026.

M. O. L. Hansen. *Aerodynamics of wind turbines*. Earthscan, London ; Sterling, VA, 2nd ed edition, 2008. ISBN 978-1-84407-438-9. OCLC: ocm86172940.

IEC. IEC TS 61400-3-2:2019 Wind energy generation systems - Part 3-2: Design requirements for floating offshore wind turbines. Technical report, 2019.

J. M. J. Journee and W. W. Massie. *Offshore Hydromechanics*. Delft University of Technlogy, Netherlands, 1st edition edition, Jan. 2001.

B. S. Kallesøe and A. M. Hansen. Dynamic Mooring Line Modeling in Hydro-Aero-ElasticWind Turbine Simulations. Hawaii, USA, 2011.

T. Kim, A. Natarajan, A. Lovera, E. Julan, C. Peyrard, M. Capaldo, G. Huwart, P. Bozonnet, and M. Guiton. A comprehensive code-to-code comparison study with the modified IEA15MW-UMaine Floating Wind Turbine for H2020 HIPERWIND project. *Journal of Physics: Conference Series*, 2265(4):042006, May 2022. ISSN 1742-6588, 1742-6596. doi: 10.1088/1742-6596/2265/4/042006. URL https://iopscience.iop.org/article/10.1088/1742-6596/2265/4/042006.

T. J. Larsen and A. M. Hansen. How 2 HAWC2, the Users Manual. Technical Report Risoe-R-1597, Forskningscenter Risoe, Risoe, Denmark, 2007.

T. J. Larsen and T. D. Hanson. A method to avoid negative damped low frequent tower vibrations for a floating, pitch controlled wind turbine. *Journal of Physics: Conference Series*, 75:012073, July 2007. ISSN 1742-6596. doi: 10.1088/1742-6596/75/1/012073. URL https://iopscience.iop.org/article/10.1088/1742-6596/75/1/012073.

Y. Liu. HAMS: A Frequency-Domain Preprocessor for Wave-Structure Interactions—Theory, Development, and Application. *Journal of Marine Science and Engineering*, 7(3):81, Mar. 2019. ISSN 2077-1312. doi: 10.3390/jmse7030081. URL https://www.mdpi.com/2077-1312/7/3/81.

F. J. Madsen, A. Pegalajar-Jurado, and H. Bredmose. Performance study of the QuLAF pre-design model for a 10 MW floating wind turbine. *Wind Energy Science*, 4(3):527–547, Sept. 2019. ISSN 2366-7451. doi: 10.5194/wes-4-527-2019. URL https://wes.copernicus.org/articles/4/527/2019/.

M. Y. Mahfouz, M. Salari, S. Hernandez, H. Bredmose, and A. Pegalajar-Jurado. D1.3 Public design and FAST models of the two 15MW floater, 2020.

S. Marelli and B. Sudret. UQLab: A Framework for Uncertainty Quantification in MATLAB. United Kingdom, 2014.

D. Moulas, M. Shafiee, and A. Mehmanparast. Damage analysis of ship collisions with offshore wind turbine foundations. *Ocean Engineering*, 143:149–162, Oct. 2017. ISSN 00298018. doi: 10.1016/j.oceaneng.2017.04.050. URL https://linkinghub.elsevier.com/retrieve/pii/S0029801817302445.

A. Ojo, M. Collu, and A. Coraddu. A Review of Design, Analysis and Optimization Methodologies for Floating Offshore Wind Turbine Substructures. *SSRN Electronic Journal*, 2021. ISSN 1556-5068. doi: 10.2139/ssrn.3936386. URL https://www.ssrn.com/abstract=3936386.

J. K. Paik and A. K. Thayamballi. *Ship-shaped offshore installations: design, building, and operation*. Cambridge University Press, 2007.

A. Pegalajar-Jurado, M. Borg, and H. Bredmose. An efficient frequency-domain model for quick load analysis of floating offshore wind turbines. *Wind Energy Science*, 3(2):693–712, Oct. 2018. ISSN 2366-7451. doi: 10.5194/wes-3-693-2018. URL https://wes.copernicus.org/articles/3/693/2018/.

A. M. Pegalajar Jurado. *Cascaded numerical models for offshore floating wind turbines*. PhD thesis, Technical University of Denmark, Denmark, 2018. URL http://orbit.dtu.dk/en/publications/cascaded-numerical-models-for-offshore-floating-wind-turbines(dad97301-979d-434a-8e76-15721b0bebb8.html. Publisher: [object Object].

C. Peyrard and Robaux. HIPERWIND D3.3: Aero-servo-hydroelastic model uncertainty, 2022.

A. C. Pillai, P. R. Thies, and L. Johanning. Comparing Frequency and Time Domain Simulations for Geometry Optimization of a Floating Offshore Wind Turbine Mooring System. In *ASME 2018 1st International Offshore Wind Technical Conference*, page V001T01A016, San Francisco, California, USA, Nov. 2018. American Society of Mechanical Engineers. ISBN 978-0-7918-5197-5. doi: 10.1115/IOWTC2018-1006. URL https://asmedigitalcollection.asme.org/OMAE/proceedings/IOWTC2018/51975/San%20Francisco,%20California,%20USA/275555.

M. Song, Z. Jiang, and W. Yuan. Numerical and analytical analysis of a monopile-supported offshore wind turbine under ship impacts. *Renewable Energy*, 167:457–472, Apr. 2021. ISSN 09601481. doi: 10.1016/j.renene.2020.11.102. URL https://linkinghub.elsevier.com/retrieve/pii/S0960148120318541.

T. Stehly and P. Duffy. 2020 Cost of Wind Energy Review. Technical Report TP-5000-81209, NREL, Golden, CO, 2021.

B. Sudret. Global sensitivity analysis using polynomial chaos expansions. *Reliability Engineering & System Safety*, 93(7):964–979, July 2008. ISSN 09518320. doi: 10.1016/j.ress.2007.04.002. URL https://linkinghub.elsevier.com/retrieve/pii/S0951832007001329.

R. Taninoki, K. Abe, T. Sukegawa, D. Azuma, and M. Nishikawa. Dynamic Cable System for Floating Offshore Wind Power Generation. *SEI Technical Review*, 2017.

A.-L. Tiberi-Wadier, A. Laugel, and M. Benoit. Construction of the Numerical Wave Databases Anemoc-2 on the Mediterranean Sea and the Atlantic Ocean Through Hindcast Simulations Over the Period 1979–2010. In P. Gourbesville, J. A. Cunge, and G. Caignaert, editors, *Advances in Hydroinformatics*, pages 127–143. Springer Singapore, Singapore, 2016. ISBN 978-981-287-614-0 978-981-287-615-7. doi: 10.1007/978-981-287-615-7_9. URL https://link.springer.com/10.1007/978-981-287-615-7_9. Series Title: Springer Water.

G. P. Van Vledder. On Wind-Wave Misalignment, Directional Spreading and Wave Loads. In *Volume 5: Ocean Engineering*, page V005T06A087, Nantes, France, June 2013. American Society of Mechanical Engineers. ISBN 978-0-7918-5539-3. doi: 10.1115/OMAE2013-11393. URL https://asmedigitalcollection.asme.org/OMAE/proceedings/OMAE2013/55393/Nantes,%20France/271561.

E. Vanem, E. Fekhari, N. Dimitrov, M. Kelly, A. Cousin, and M. Guiton. A Joint Probability Distribution Model for Multivariate Wind and Wave Conditions. In *Volume*

2: Structures, Safety, and Reliability, page V002T02A013, Melbourne, Australia, June 2023. American Society of Mechanical Engineers. ISBN 978-0-7918-8684-7. doi: 10.1115/OMAE2023-101961. URL https://asmedigitalcollection.asme.org/OMAE/proceedings/OMAE2023/86847/V002T02A013/1166968.

D. N. Veritas. Recommended Practice DNV-RP-C203 Fatigue design of offshore steel structures. Technical report, Apr. 2010.

B. Yildirim, N. Dimitrov, A. B. Abrahamsen, and A. Kolios. A reduced order/simplified method for uncertainty quantification on the floating wind turbine design basis. *Journal of Physics: Conference Series*, 2024.

Z. Yu, J. Amdahl, M. Rypestøl, and Z. Cheng. Numerical modelling and dynamic response analysis of a 10 MW semi-submersible floating offshore wind turbine subjected to ship collision loads. *Renewable Energy*, 184:677–699, Jan. 2022. ISSN 09601481. doi: 10.1016/j.renene.2021.12.002. URL https://linkinghub.elsevier.com/retrieve/pii/S0960148121017213.

S. Zhou, K. Müller, C. Li, Y. Xiao, and P. W. Cheng. Global sensitivity study on the semisubmersible substructure of a floating wind turbine: Manufacturing cost, structural properties and hydrodynamics. *Ocean Engineering*, 221:108585, Feb. 2021. ISSN 00298018. doi: 10.1016/j.oceaneng.2021.108585. URL https://linkinghub.elsevier.com/retrieve/pii/S0029801821000202.